Nanoscale Torsional Dissipation Dilution for Quantum Experiments and Precision Measurement

J. R. Pratt,[1,*] A. R. Agrawal,[2,*] C. A. Condos,[2,*] C. M. Pluchar,[2,*] S. Schlamminger,[1] and D. J. Wilson[2,†]

[1]National Institute of Standards and Technology, 100 Bureau Drive, Gaithersburg, Maryland 20899, USA
[2]Wyant College of Optical Sciences, University of Arizona, Tucson, Arizona 85721, USA

(Received 24 May 2022; accepted 22 December 2022; published 15 February 2023)

The quest for ultrahigh-Q nanomechanical resonators has driven intense study of strain-induced dissipation dilution, an effect whereby vibrations of a tensioned plate are effectively trapped in a lossless potential. Here, we show for the first time that torsion modes of nanostructures can experience dissipation dilution, yielding a new class of ultrahigh-Q nanomechanical resonators with broad applications to quantum experiments and precision measurement. Specifically, we show that torsion modes of strained nanoribbons have Q factors scaling as their width-to-thickness ratio squared (characteristic of "soft clamping"), yielding Q factors as high as 10^8 and Q-frequency products as high as 10^{13} Hz for devices made of Si_3N_4. Using an optical lever, we show that the rotation of one such nanoribbon can be resolved with an imprecision 100 times smaller than the zero-point motion of its fundamental torsion mode, without the use of a cavity or interferometric stability. We also show that a strained nanoribbon can be mass loaded without changing its torsional Q. We use this strategy to engineer a chip-scale torsion pendulum with an ultralow damping rate of 7 μHz and show how it can be used to sense micro-g fluctuations of the local gravitational field. Our findings signal the potential for a new field of imaging-based quantum optomechanics, demonstrate that the utility of strained nanomechanics extends beyond force microscopy to inertial sensing, and hint that the landscape for dissipation dilution remains largely unexplored.

DOI: 10.1103/PhysRevX.13.011018

Subject Areas: Condensed Matter Physics, Gravitation, Quantum Physics

I. INTRODUCTION

Recent years have seen the emergence of a new class of ultrahigh-Q mechanical resonators fashioned from strained thin films [1]. The mechanism behind their performance is dissipation dilution, an effect whereby an elastic body is subjected to a conservative stress field, increasing its stiffness without adding loss [2,3]. Access to extreme dimensions and stresses at the nanoscale has enabled dilution factors (the ratio of final to initial Q) in excess of 10^5, yielding Q factors in excess of 10^9 for devices made of amorphous glass and Q-frequency products exceeding 10^{15} Hz using "soft clamping" [4,5]. Attractive features of these devices include attonewton force sensitivities [6], thermal coherence times of milliseconds [4], and zero-point displacement amplitudes in excess of picometers [5], spurring proposals from room-temperature quantum experiments [7] to ultrafast force microscopy [8].

Despite rapid innovation, a key limitation of dissipation dilution is its restriction to transverse flexural modes, a consequence of its reliance on nonlinear stress-strain coupling. It has been formally shown [3] that breathing modes, such as the longitudinal modes of a cylinder, cannot be diluted by a uniform strain field, ruling out the application of dissipation dilution to a large class of metrologically important mechanical devices, such as the mirrors used in precision optical cavities and gravitational wave interferometers. It is also commonly held that torsion modes of nanostructures are not diluted by strain [3,9,10], despite the prevalence of tensioned microsuspensions in macroscopic torsion pendula [11] and the historic use of torsion microresonators to study mechanical loss [12].

Here, we show that torsion modes of a simple nanobeam can experience massive dissipation dilution due to thin film stress and draw a connection to a century-old theory from the torsion balance community [13] that implies that torsion modes of a beam are naturally soft-clamped [4]. The key insight is that, when tensioned, the torsional stiffness of a beam increases as its width-to-thickness-ratio w/h squared; thus, for ribbonlike nanobeams (not commonly studied in nanomechanics [14]), torsional Q factors should scale as

*These authors contributed equally to this work.
†Corresponding author.
dalziel@arizona.edu

$(w/h)^2$, provided that curvature at the clamps is negligible. We confirm this theory by studying high-stress Si_3N_4 nanoribbons with w/h as high as 10^4, realizing Q factors as high as 10^8 and Q-frequency products as high as 10^{13} Hz at room temperature.

By resolving a common misperception in the nanomechanics community (that torsion modes do not experience dissipation dilution [3]), our findings invite a rethinking of strategies for quantum experiments and precision measurement with nanomechanical resonators. We explore two examples: First, owing to their large angular zero-point motion, strained nanoribbons are promising for imaging-based quantum optomechanics [15–17]. We show this by resolving the rotation of a Si_3N_4 nanoribbon with an imprecision 100 times smaller than its peak zero-point spectral density using an optical lever, setting the stage for observation of radiation pressure shot noise in torque [18]. Second, with precision inertial sensing in mind, we show that strained nanoribbons can be mass loaded without reducing their torsional Q (contrary to what is typically observed for flexural modes [19,20]). We use this strategy to engineer chip-scale torsion pendula with damping rates as low as 7 μHz and describe how such a device can be used to sense micro-g fluctuations of local gravity.

The remainder of the paper provides an essential overview of these findings, followed by the Appendix with key derivations. Comprehensive theoretical and experimental discussion is provided in Supplemental Materials [21].

II. BIFILAR SUSPENSIONS AND TORSIONAL DISSIPATION DILUTION

The history of torsional dissipation dilution can be traced back to the theory of bifilar suspensions by Buckley in 1914 [13]. In brief, loading a torsion strip with a massive plumb bob increases its stiffness without adding loss [11]. This is because, as the strip twists, it lifts the bob and does work against a conservative gravitational field. Vibrating in its fundamental mode, the Q of the loaded strip scales as the ratio of its torsional stiffness due to tensile (k_σ) and internal stress (k_E) [21]:

$$\frac{Q}{Q_0} = 1 + \frac{k_\sigma}{k_E} \approx \frac{\sigma}{2E}\left(\frac{w}{h}\right)^2, \tag{1}$$

where w and h are the strip width and thickness, respectively, $\sigma = mg/wh$ is the tensile stress due to gravity (Fig. 1), and E is the elastic modulus of the strip material.

Generalized dissipation dilution theory [3] holds that any form of static tensile stress, such as residual stress in thin films, can give rise to dissipation dilution. Buckley's theory can therefore be generalized to the idea that *placing a ribbon under tensile stress increases its stiffness without adding loss*. Equation (1) should, thus, hold for a nanoribbon released from a thin film with biaxial stress σ. Remarkably, Eq. (1) is also known to be the ideal "soft-clamped" dissipation dilution factor for a thin beam vibrating in its fundamental flexural mode (with width replaced by half length) [5]. In the Appendix, we provide a continuum mechanics model that supports this claim, which we now proceed to investigate experimentally.

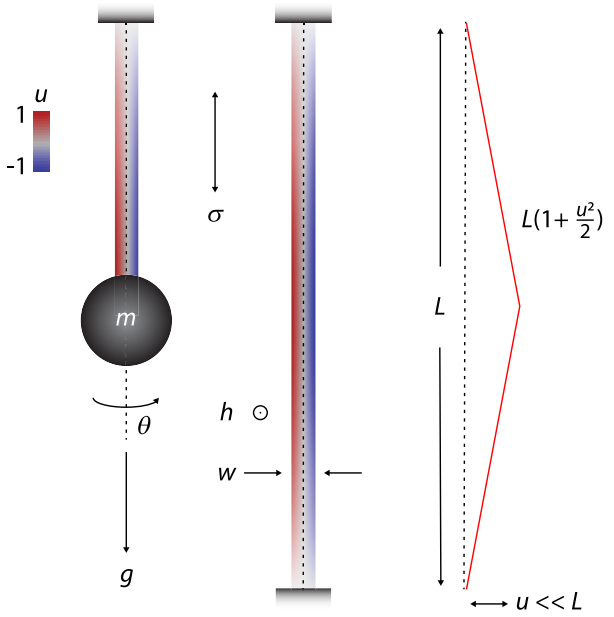

FIG. 1. Dissipation dilution of a torsion resonator. Left: a torsion pendulum formed by suspending a mass m from a ribbonlike fiber of width w and thickness h. Gravity loads the fiber into tension mg, producing a tensile stress $\sigma = mg/wh$. The color gradient represents the transverse displacement u of the fundamental torsion mode. Center: a doubly clamped ribbon under tensile prestress σ. Right: bifilar model of the ribbon's torsion mode [21]. In both cases, the ribbon length L is preserved to first order, leading to dissipation dilution.

III. TORSIONAL DISSIPATION DILUTION OF Si_3N_4 NANORIBBONS

To investigate Eq. (1), we fabricated a set of high-stress Si_3N_4 nanoribbons with aspect ratios w/h varying from 10^2 to 10^4 [21] [Fig. 2(a)]. Devices were housed in a room-temperature high-vacuum chamber ($\lesssim 10^{-7}$ mbar), and ringdowns [Fig. 2(c)] were performed using optical lever measurements in conjunction with radiation pressure driving [21]. Ringdown-inferred Q factors were then compiled for flexural and torsional modes up to third order, as shown in Fig. 2(d) and Supplemental Material [21].

Considering first the hypothesis that $Q \propto (w/h)^2$, in Fig. 2(d) we compare Q factors of ribbons with widths from 10 to 400 μm to the lumped mass model [Eq. (1)] and a finite element model accounting for bending loss at the clamps [21]. For both models, we assume $\sigma = 0.85$ GPa [21], $E = 250$ GPa, $h = 75$ nm, and $Q_0 = 6000 \times h/(100\ \text{nm})$ (an established surface loss model for Si_3N_4 thin film resonators [22]). We observe quantitative

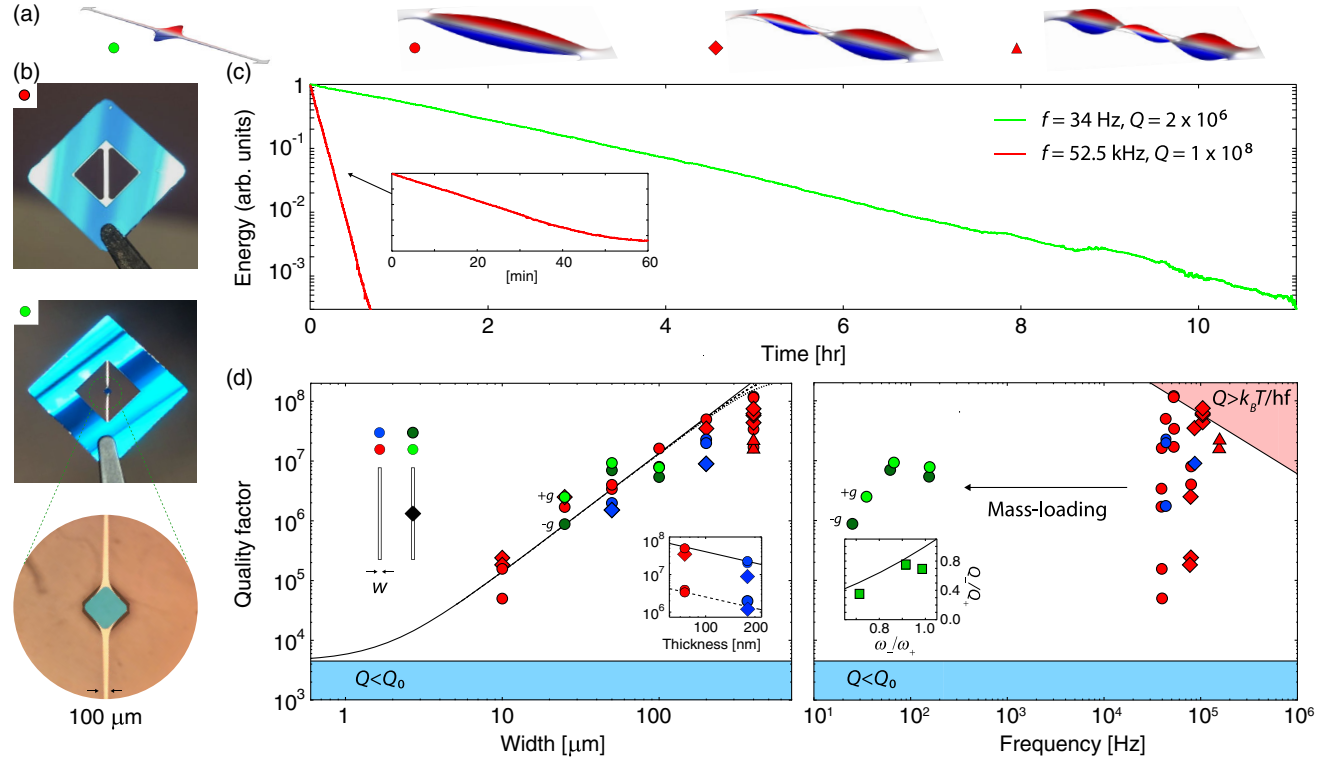

FIG. 2. Ultralow-loss nanomechanical torsion resonators. (a) Simulated torsion modes of a nanoribbon with (green) and without (red) mass loading. (b) Photos of representative devices: (top) a 400-μm-wide, 7-mm-long, 75-nm-thick ribbon; (middle) a 25-μm-wide, 7-mm-long, 75-nm-thick ribbon loaded with a 100-μm-thick Si paddle; and (bottom) a micrograph of the paddle. (c) Ringdowns of the fundamental mode of a 400-μm-wide ribbon (red) and a mass-loaded, 25-μm-wide ribbon (green). (d) Compilation of Q versus ribbon width (left) and frequency (right). Red and blue points correspond to thicknesses of 75 and 180 nm, respectively. Dark and light green points correspond to inverted ($-g$) and noninverted ($+g$) chip orientations, respectively. Solid, dashed, and dotted curves correspond to the lumped mass model, finite element model, and a gas damping model with $Q_{\mathrm{gas}} = 1.1 \times 10^9$ [21], respectively. Left inset: Q versus thickness for 200- and 50-μm-wide beams, compared to the lumped model (solid and dashed lines). Right inset: Q versus frequency for mass-loaded ribbons of different orientation, compared to Eq. (4) (solid line).

agreement up to a width of 100 μm, beyond which Q begins to drop, consistent with simulated bending loss [21] and gas damping (we estimate $Q_{\mathrm{gas}} \approx 10^9$ [21]). For widths smaller than 100 μm, we observe a slightly higher Q than predicted by both models. Though a more careful investigation is required, we speculate this may be due to an overestimate of surface loss, since the model in Ref. [22] is inferred from a study of flexural rather than torsional modes.

Further support for Eq. (1) was obtained by inspecting higher-order modes [solid diamonds and triangles in Figs. 2(d) and 2(e)]. The continuum model derived in the Appendix predicts that Q_n/Q_0 is independent of mode order n for acoustic wavelengths $L/n \gg w$, consistent with our observation that $\{Q_n\}$ is bound above by Eq. (1). We also observed that the fundamental torsional mode had consistently high Q. This is contrary to the typical behavior of flexural modes of Si_3N_4 beams and membranes [22] and suggests that torsional modes may be more resistant to acoustic radiation ("mounting") loss [23].

Finally, we fabricated several ribbons with a different thickness, 180 nm, and observed that the Q of torsion modes scaled inversely with thickness [Fig. 2(d) inset]. By contrast, as shown in Supplemental Material [21], we observed that the Q of flexural modes were roughly independent of width and thickness. These different scalings are telltale signatures of soft clamping ($Q/Q_0 \propto w^2/h^2$) and "hard clamping" ($Q/Q_0 \propto w/h$) [14], respectively, in the presence of surface loss ($Q_0 \propto h$) [22].

IV. QUANTUM-LIMITED DEFLECTOMETRY OF A NANORIBBON

Nanomechanical resonators have been probed at the quantum limit using cavity-enhanced interferometry [24,25]. In principle, however, neither a cavity nor interferometry is necessary, provided that the measurement is optimally efficient [26]. Owing to their high torsional Q, strained nanoribbons present a unique opportunity to study the quantum limits of deflectometry, a measurement technique of long-standing inquiry in the field of quantum imaging [27,28] which has received relatively little attention from the quantum optomechanics community [29]. Pursuing an established benchmark [30,31], in our study

of Si_3N_4 nanoribbons, we found that the imprecision of optical lever measurements S_θ^{imp} [here, expressed as a power spectral density evaluated at mechanical resonance $S_\theta(\omega_0) \equiv S_\theta$] could be reduced far below the zero-point angular displacement of the ribbon's fundamental torsion mode S_θ^{ZP}, satisfying a basic requirement for displacement measurement at the standard quantum limit (at the "SQL," $S_\theta^{\mathrm{imp}} = S_\theta^{\mathrm{BA}} = S_\theta^{\mathrm{ZP}}/2$, where S_θ^{ba} is the displacement produced by backaction torque $S_\tau^{\mathrm{BA}} \geq \hbar^2/S_\theta^{\mathrm{imp}}$) [16,18,30]. To our knowledge, this represents the first deflectometric displacement measurement with an imprecision below that at the SQL ($S_\theta^{\mathrm{imp}} < S_\theta^{\mathrm{ZP}}/2$) [30]. Combined with the high Q-f products of our devices (exceeding the threshold for quantum coherence at room temperature, $Qf = k_B T/h > 6 \times 10^{12}$ Hz [32]), access to sub-SQL deflection measurements signals the potential for a new generation of imaging-based quantum optomechanics experiments [15–17], in which thermal motion is overwhelmed by radiation pressure shot noise in torque.

To explore the potential for torsional quantum optomechanics, we revisit the optical lever technique with an eye to maximizing the ratio $S_\theta^{\mathrm{ZP}}/S_\theta^{\mathrm{imp}}$ for a torsion ribbon. As shown in Fig. 3(a), the "lever" is formed by reflecting a laser beam off the ribbon and monitoring its deflection on a split photodiode. In the far field, angular displacement of the ribbon θ can be resolved with a shot-noise-limited imprecision of [21,28,33]

$$S_\theta^{\mathrm{imp}} \gtrsim \frac{1}{w_0^2}\frac{\hbar c \lambda}{8 P \eta}, \tag{2}$$

where w_0 and P are the waist size and reflected power of the laser beam, respectively, and $\eta \in [0, 1]$ is an efficiency parameter accounting for optical loss and imperfect transduction. Comparing to the zero-point displacement spectral density of the ribbon's fundamental torsion mode [21]

$$S_\theta^{\mathrm{ZP}} = \frac{1}{w^2}\frac{8\hbar Q_1}{m_1 \omega_1^2} \tag{3}$$

(quality factor $Q_1 \propto w^2/h^2$, effective mass $m_1 = \rho h w L/6$, and frequency $\omega_1 \propto \sqrt{\sigma/L^2}$ [21]), we find that maximum "leverage" is achieved by matching the widths of the laser beam and the ribbon ($w_0 \approx w/2$), giving access to a favorable scaling $S_\theta^{\mathrm{ZP}}/S_\theta^{\mathrm{imp}} \propto Q_0 w/h^3$ due to dissipation dilution.

An optical lever measurement with an imprecision below that at the SQL [30,31] is shown in Fig. 3. The measurement was made by reflecting a $w_0 \approx 200$-μm-wide laser beam from a 400-μm-wide, 75-nm-thick nanoribbon and detecting the 4 mW reflected field at a distance of 0.4 m. The lateral position of the split photodetector was trimmed to balance out classical intensity noise, and the ribbon position was trimmed to optimize coupling to the fundamental torsion mode [21]. Near the fundamental

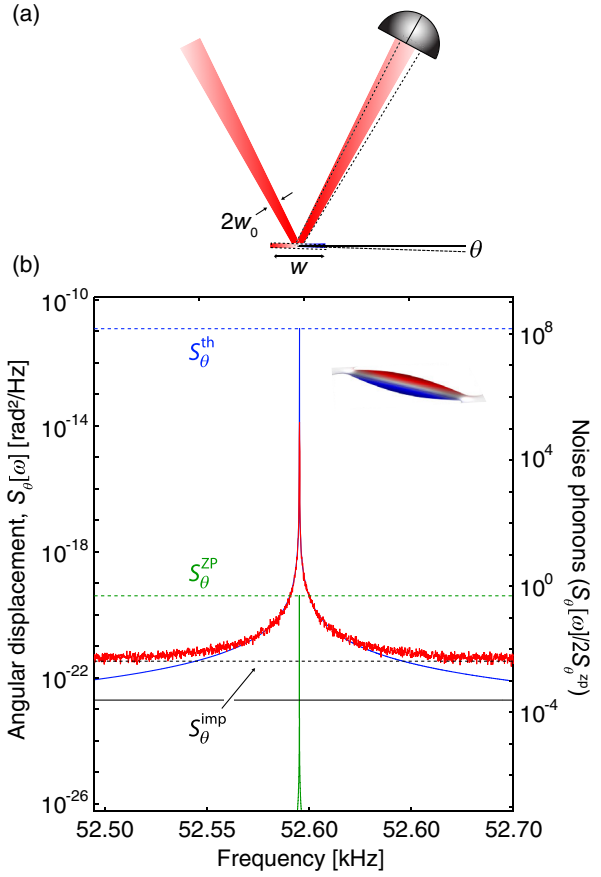

FIG. 3. Optical lever measurement with an imprecision below that at the standard quantum limit. (a) Schematic of the optical lever technique: A Gaussian beam with waist w_0 is reflected off a torsion ribbon of width w (the beam waist is at the ribbon [21]). Ribbon deflection θ is monitored using a split photodiode. (b) Displacement of a $w = 400$ μm ribbon measured using a $w_0 \approx 200$ μm, $P = 4$ mW optical lever. Solid curves correspond to data (red), a thermal noise model (blue), and the inferred zero-point spectral density [21] (green). Dotted lines are guides to the eye for the peak thermal (blue), zero-point (green), and imprecision (black) noise. The ideal imprecision [Eq. (2) with $\eta = 1$] is shown as a solid black line.

torsional resonance frequency, $\omega_1 \approx 2\pi \times 52.5$ kHz, the photocurrent spectrum is dominated by thermal noise with a peak magnitude of $S_\theta^{\mathrm{th}} = 2n_{\mathrm{th}} S_\theta^{\mathrm{ZP}}$, well in excess of zero-point motion due to the large thermal mode occupation, $n_{\mathrm{th}} = k_B T/\hbar\omega_1 \approx 1.4 \times 10^8$ (accounting for a small amount of photothermal heating, $T \approx 350$ K [21]). Fitting the noise peak to a Lorentzian $S_\theta[\omega] = S_\theta^{\mathrm{imp}} + S_\theta^{\mathrm{th}}/[1 + 4Q_1^2(\omega - \omega_1)^2/\omega_1^2]$, with $Q_1 = 8.5 \times 10^7$ determined by ringdown, we infer that the measurement imprecision S_θ^{imp} is a factor of 120 below the zero-point spectral density S_θ^{ZP} and a factor of 17 above the ideal value implied by Eq. (2). While this inference is independent of modal mass ($m_1 \approx 0.1$ μg), we speculate that the hierarchy $S_\theta^{\mathrm{ZP}} \gg S_\theta^{\mathrm{imp}}$ is aided by the large magnitude of the zero-point motion $S_\theta^{\mathrm{ZP}} \approx (0.5\ \mathrm{nrad}/\sqrt{\mathrm{Hz}})^2$ and the

immunity of deflectometry to various forms of technical noise.

V. A CHIP-SCALE TORSION PENDULUM GRAVIMETER

Mass loading a micromechanical resonator is the basis for chip-scale inertial sensing; however, it typically entails increasing mechanical loss, leading to complicated size-sensitivity trade-offs [19,20]. In our study of Si_3N_4 nanoribbons, we found that mass loading them with a central Si pad (originally a fabrication artifact) had little effect on their torsional Q, enabling us to realize chip-scale torsion pendula with Q-m products as high as kilograms and damping rates as low as microhertz. Owing to their significant gravitational stiffness, these devices can, in fact, possess higher Q than unloaded ribbons, due to gravitational dissipation dilution. They also show promise as chip-scale pendulum gravimeters, achieving spectral resolutions of several micro-g for first-generation devices.

In Fig. 2, we present a study of three mass-loaded nanoribbons (green) alongside unloaded ribbons (red). Each ribbon is 75 nm thick with a width of $w = 25$, 50, or 100 μm. To load the ribbon, as shown in Fig. 2(b), a central defect is intentionally underetched [21], producing a 100-μm-thick, 600×600-μm^2-wide Si pad with mass $m_{pad} \approx 0.1$ mg. As shown in Fig. 2(d) (right), optical lever measurements of these devices revealed an approximately thousandfold drop in the fundamental torsion mode frequency from 50 kHz to 34 ($w = 25$ μm), 70 (50 μm), and 150 Hz (100 μm), respectively, corresponding to a millionfold increase in moment of inertia. Despite this substantial mass loading, ringdown measurements of the 25 and 50 μm devices revealed an *increased* Q (2.5×10^6 and 1.0×10^7) relative to unloaded ribbons (1.5×10^6 and 4×10^6), corresponding to damping rates of $\Delta\omega/(2\pi) = 14$ and 7 μHz and Q-m products of 0.25 and 1.0 kg, respectively.

The reduced frequency and increased Q of the "torsion micropendula" in Fig. 2 suggest that their dynamics are strongly influenced by the local acceleration of gravity g. To confirm this, as shown in Fig. 4, the pendula were inverted and their frequency and Q were compared to the lumped mass model:

$$\omega_{\pm} = \sqrt{(k_E + k_\sigma \pm k_g)/I}, \tag{4a}$$

$$Q_{\pm} = Q_0\left(1 + \frac{k_\sigma \pm k_g}{k_E}\right) = Q_{\mp}\left(\frac{\omega_{\mp}}{\omega_{\pm}}\right)^2, \tag{4b}$$

where $k_g = m_p g h_p/2$ and I are the gravitational stiffness and moment of inertia of the pad (mass m_p and thickness h_p), respectively, and $-(+)$ indicates the inverted (noninverted) orientation. As shown in Figs. 4(c) and 4(d), for the softest, $\omega_+/(2\pi) = 35$ Hz ($w = 25$ μm) pendulum, inversion resulted in a 10 Hz drop in resonance frequency

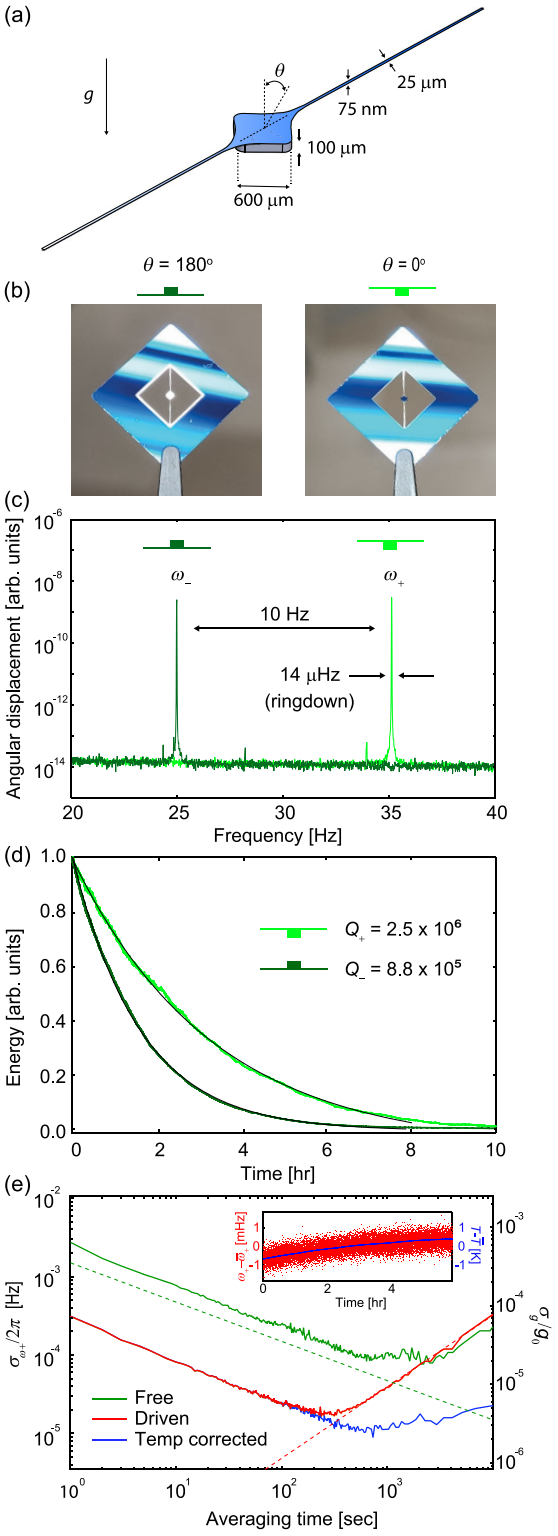

FIG. 4. Torsion micropendulum gravimeter. (a) Device geometry: a Si_3N_4 nanoribbon (blue) loaded with a Si pad (gray). (b) Photographs, (c) displacement spectra, and (d) ringdowns of the device in inverted and noninverted configuration. (e) Free-running (green), driven (red), and temperature-corrected (blue) Allan deviation measurements. Inset: frequency (red) and temperature (blue) of driven device. Dashed lines: thermal noise (green) and drift (red) model.

$(\omega_-/\omega_+ = 0.71)$ and a threefold drop in Q factor $(Q_-/Q_+ = 0.35)$, in good agreement with Eq. (4) for $k_g \approx k_\sigma \approx 200k_E$. Similar agreement was observed for wider, stiffer ribbons, as highlighted by the inset in Fig. 2(e).

Owing to their large Q-k_g product, it is intriguing to consider using mass-loaded Si_3N_4 nanoribbons as pendulum "clock" gravimeters. The potential of our first-generation devices can be seen by noting that their spectral resolution to gravity (the gravity change producing a frequency shift equal to the pendulum damping rate) is at the micro-g level, viz.

$$\Delta g = \left(\frac{d\omega_+}{dg}\right)^{-1}\Delta\omega_+ \approx \frac{4g_0}{Q_+}\frac{\omega_+^2}{\omega_+^2-\omega_-^2} \approx \frac{2g_0}{Q_0}\frac{k_E}{k_g} \sim 10^{-6}g_0, \tag{5}$$

where g_0 is standard gravity. This resolution can be improved by driving the pendulum and averaging its frequency, yielding an ideal thermal-noise-limited Allan deviation [34,35] of

$$\sigma_g(\tau) = \left(\frac{d\omega_+}{dg}\right)^{-1}\sigma_{\omega_+}(\tau) = \Delta g\sqrt{\frac{\tau_+}{\epsilon\tau}}, \tag{6}$$

where τ is the averaging time, $\sigma_{\omega_+} = \Delta\omega_+\sqrt{\tau_+/(\epsilon\tau)}$ and $\tau_+ = \Delta\omega_+^{-1}$ are the frequency Allan deviation and energy damping time of the pendulum, respectively, and $\epsilon = \langle\theta^2\rangle/\langle\theta_{\rm th}^2\rangle$ is the ratio of the driven to thermal energy.

To explore its potential as a gravimeter, the 34 Hz pendulum shown in Fig. 4 was mounted on a 1 Hz vibration isolation stage (atop a floated optical table), and its resonance frequency was tracked using a digital algorithm [21]. Allan deviations were then recorded with the device free running (green) and in free decay (red, with an energy ringdown time of $\tau_+ = 1.1\times10^4$ s) after an impulsive radiation pressure drive. As shown in Fig. 4(e), the free-running Allan deviation was within a factor of 2 of the thermal noise limit $\sigma^{\rm th}_{\omega_+}(\tau) = \Delta\omega_+\sqrt{\tau_+/\tau}$ [36] (dashed green), for averaging times $\tau \lesssim 1000$ s, saturating at $\sigma_{\omega_+}/2\pi \approx 70$ μHz and a gravity resolution of $\sigma_g = \Delta g\sqrt{\tau_+/\tau} \approx 20\mu g_0$. The driven Allan deviation was 10 times lower, reaching $\sigma_{\omega_+}/2\pi \approx 18$ μHz ($\sigma_g \approx 4$ μg) at 300 s; however, both cases are limited by a frequency drift of $d\omega_+/d\tau \approx 2\pi\times 0.3$ mHz/h at late times (dashed red). As shown in the inset, we find this drift to be well correlated with the 0.3 K/h temperature drift of the device holder, implying a frequency sensitivity of $d\omega_+/dT \approx 2\pi\times 1$ mHz/K. The blue curve in Fig. 4(e) is obtained by subtracting a scaled temperature measurement [21], yielding $\sigma_{\omega_+}/2\pi \approx 12$ μHz ($\sigma_g \approx 2.5$ μg) at $\tau \approx 800$ s.

VI. SUMMARY AND OUTLOOK

In summary, we studied high-stress Si_3N_4 nanoribbons with width-to-thickness (w/h) ratios as large as 10^4 and found that their torsion modes experienced dissipation dilution scaling as $(w/h)^2$, yielding Q factors as high as 10^8 and Q-f products as high as 10^{13} Hz. Owing to their large zero-point angular displacement $S_\theta^{\rm ZP} \sim (\text{nrad}/\sqrt{\text{Hz}})^2$, these devices are promising for quantum-limited deflectometry studies. We demonstrated this by showing that an optical lever measurement could resolve the rotation of a nanoribbon with an imprecision 20 dB smaller than its zero-point motion, paving the way for the investigation of radiation pressure shot noise in torque. We also found that strained nanoribbons could be mass loaded without reducing their torsional Q, enabling us to fabricate chip-scale torsion pendula with damping rates as low as 7 μHz and Q-m factors as high as 1 kg. We explored how these devices might be used as "clock" gravimeters, achieving a resolution of several micro-g in 10 min, limited by thermal drift.

Looking forward, we highlight several routes to improvement. Starting with the devices themselves, we note that the $Q \sim (w/h)^2$ soft-clamping behavior of nanoribbons [Fig. 2(d)] is highly sensitive to clamp geometry. Our use of diagonal fillets was inspired by optimized Si_3N_4 nanotrampolines [6,37]; as discussed in Supplemental Material [21], this choice turns out to be serendipitous, as square fillets [38] and unfilleted ribbons would have experienced increased bending loss and even buckling [39] beyond $w > 100$ μm, according to simulations (Fig. S3). Confirming this behavior and exploring routes to further clamp optimization—a task which seems ripe for an emerging set of optimization algorithms [40,41]—will be important to realizing $Q > 10^8$ devices. The robustness of torsion modes of nanoribbons to anchor loss [42], mass loading [20], and surface loss [22] is also an open question, with potential for substantial improvement over flexural modes.

With regards to deflectometry-based quantum optomechanics, a key next step will be to search for motion due to radiation pressure shot noise in torque, $S_\theta^{\rm BA} \simeq (S_\theta^{\rm ZP})^2/S_\theta^{\rm imp}$ [18]. Starting with the measurement in Fig. 3, for which $S_\theta^{\rm BA}/S_\theta^{\rm th} \sim 10^{-4}$, a hypothetical route to $S_\theta^{\rm BA}/S_\tau^{\rm th} \sim 1$ would be to precool the nanoribbon to 4 K, decrease its mass by a factor of 10 (e.g., by thinning and shortening the ribbon), and increase the reflected optical power by 10 dB, leveraging reduced absorption at telecommunications wavelengths [43], a photonic crystal mirror [44], and/or cavity enhancement [45], to mitigate photothermal heating. An alternative approach would be to look for signatures of $S_\theta^{\rm BA}$ in optomechanical quantum correlations [46], which in principle could be discerned with $S_\theta^{\rm BA} \ll S_\theta^{\rm th}$. Interestingly, for an optical lever measurement, the correlations are produced between the angular and lateral displacement of the deflected beam (or, equivalently, the HG_{00} and HG_{01} components of the deflected beam) [16] rather than phase

and amplitude as in the case of an interferometric measurement [47]. While such spatial mode squeezing has been realized in multimode quantum optics experiments [15], it has only recently been explored in the optomechanical domain [48] and offers fertile analogies to ponderomotive squeezing [47].

Finally, to improve the performance of mass-loaded Si_3N_4 nanoribbons as gravimeters, it will be important to study their frequency stability. A natural target is $\sigma_g < 10^{-6} g_0$, which for the device in Fig. 4 could, in principle, be achieved with tenfold larger drive amplitude $\sqrt{\epsilon}$ or tenfold smaller drift. The corresponding fractional Allan deviation $\sigma_{\omega_+}/\omega_+ \lesssim 10^{-7}$ has been widely achieved with megahertz flexural modes of Si_3N_4 nanobeams [34,36,49,50]; however, it is an open question whether the lower frequency of our mass-loaded devices will pose new challenges. One constraint, on ϵ, is the intrinsic spring-softening nonlinearity of the pendulum ($k_g \propto \cos\theta$), which, in principle, might be compensated by the Duffing nonlinearity of the nanoribbon [21]. With regards to drift, we note that the temperature sensitivity $d\omega_+/dT$ of our devices agrees well with the predicted strain sensitivity $d\sigma/dT$ of the Si_3N_4 nanoribbon due to thermal expansion mismatch with the Si substrate [21,49]. Thermally invariant strain engineering has been used to reduce this source of drift by 2 orders of magnitude [49] and could be directly applied here. A compelling alternative would be to fabricate the nanoribbon from single-crystal strained Si [51], which could also enable higher Q_0, especially at cryogenic temperatures. Ultimately, a combination of these strategies may be necessary to compete with state-of-the-art $\sigma_g \sim$ 10 ng MEMS gravimeters [52–54]; nevertheless, the large dynamic range ($\pm 2g_0$, enabled by the lossless tensile stiffness $k_\sigma > k_g$), submilligram mass, and exceptional simplicity of the micropendulum approach invites further investigation.

ACKNOWLEDGMENTS

This work is supported by the National Science Foundation (NSF) Convergence Accelerator Program under Grant No. 2134830. D. J. W. acknowledges additional support from NSF Grant No. ECCS-1945832 and from the Northwestern University Center for Fundamental Physics and the John Templeton Foundation through a Fundamental Physics grant. J. R. P. and S. S. are grateful to the NIST Calibration Services Development fund and the Fundamental Electronic Measurements group for support of their work on this project. C. M. P. acknowledges support from an Amherst College Fellowship, an ARCS Foundation Scholarship, and a Grant in Aid of Research from Sigma Xi; A. R. A. acknowledges support from a CNRS-UArizona iGlobes fellowship; and C. A. C. acknowledges support from a Friends of Tucson Optics Endowed Scholarship. Finally, the reactive ion etcher used for this study was funded by an NSF MRI grant, ECCS-1725571.

J. R. P. conceived of the project, including anticipating torsional dissipation dilution in strained nanoribbons and applying this effect to chip-scale gravimetry. A. R. A. fabricated the original mass-loaded nanoribbon (inspiring J. R. P.'s conception of the project) and conducted all fabrication and numerical simulation of later devices. C. A. C. led the development of apparatuses for characterizing unloaded, and, separately, mass-loaded nanoribbons, conducted most of the ringdown measurements of both devices, and took all measurements presented in the gravimetry section. C. M. P. conceived of the quantum-limited deflectometry experiment, refined the optical lever apparatus for this purpose, took all optical lever measurements presented in the main text and Supporting Materials, and developed and applied the theory for analyzing them. D. J. W. developed the continuum mechanics model for torsional dissipation dilution and co-analyzed all measurements. J. R. P. and D. J. W. co-wrote the manuscript with assistance from all co-authors. All authors co-wrote the Supporting information. S. S. provided expert advice on all aspects of the experiment and theory. J. R. P. and D. J. W. oversaw the project.

APPENDIX

In this appendix, we provide condensed derivations of Eqs. (1)–(3). Extended derivations and comprehensive experimental details are provided in Supplemental Material.

1. Torsional dissipation dilution

a. Lumped mass model

The Zener model of dissipation treats internal modes of an elastic body as a mass suspended from a spring-dashpot system modeled by a complex spring constant $k = k_0(1 + iQ_0^{-1})$. The Q factor of the mode is then given by $Q_0 = \mathrm{Re}[k]/\mathrm{Im}[k]$. In this lumped mass approach, dissipation dilution is modeled as a lossless (real-valued) spring k' added in parallel to the lossy (complex) spring, yielding a renormalized Q factor

$$Q = \frac{\mathrm{Re}[k + k']}{\mathrm{Im}[k + k']} = Q_0\left(1 + \frac{k'}{k_0}\right). \tag{A1}$$

To derive Eq. (1), we use the ansatz that loading a ribbon into tensile stress increases its torsional stiffness without adding loss. The stiffness of an unstressed ribbon is attributable to Saint-Venant [55] and is given by

$$k_E = \frac{Eh^3 w}{6l}, \tag{A2}$$

where $2l$ is the ribbon length. The stiffness of a tensioned ribbon can be traced to the bifilar theory of Buckley [13]:

$$k_\sigma = \frac{\sigma h w^3}{12 l}. \tag{A3}$$

Equation (1) is given by setting $k_0 = k_E$ and $k' = k_\sigma$.

b. Continuum model

A continuum mechanics model for dissipation dilution of an elastic body is provided in Ref. [3] and recounted in Supplemental Material. In this model, the Q factor of a vibrational mode is related to the time-varying strain field it produces, viz.,

$$\frac{Q}{Q_0} = 1 + \frac{\int \bar{\epsilon}_{ij} \langle \Delta\epsilon_{ij} \rangle dV}{\frac{1}{2}\int \langle \Delta\epsilon_{ij} \Delta\epsilon_{ij} \rangle dV}, \tag{A4}$$

where (using Cartesian coordinates and index notation)

$$\epsilon_{ij} = \frac{1}{2}(\partial_i u_j + \partial_j u_i + \partial_i u_k \partial_j u_k) = \bar{\epsilon}_{ij} + \Delta\epsilon_{ij}(t) \tag{A5}$$

is the time-varying strain tensor and

$$u_i(\vec{r}, t) = \sum_n \phi_i(\vec{r}) A e^{i\omega_0 t} \tag{A6}$$

is the time-varying displacement field of the mode with amplitude A, eigenfrequency ω_0, and mode shape ϕ_i.

To derive Eq. (1), we assume a mode shape of the form

$$\phi_\theta(z) = \sin(k_1 z) - k_1 L \lambda (e^{-z/(\lambda L)} - 1), \tag{A7}$$

where θ denotes the angle of rotation about the ribbon axis z, $k_1 = \pi/L$, and $\lambda L \equiv h\sqrt{E/12\sigma}$ characterizes the rapidly varying mode curvature at the clamps [$\phi_\theta(z)$ is obtained by solving the Euler-Bernoulli equation with boundary conditions $\phi_\theta(z) = [\phi_\theta(z)]'_z = 0$ [3]]. Following the torsion theory of Saint-Venant [55] with $\phi_\theta \ll 1$ and "warping function" $W(x, y) \approx -xy$ [appropriate for a thin beam ($h \ll w$) with a constant twist rate $(u_\theta)'_z = 0$], the mode shape can be expressed in Cartesian coordinates as [56–58]

$$\phi_x(x, y, z) = -y\phi_\theta(z), \tag{A8a}$$

$$\phi_y(x, y, z) = x\phi_\theta(z), \tag{A8b}$$

$$\phi_z(x, y, z) = W(x, y)[\phi_\theta(z)]'_z \approx -xy[\phi_\theta(z)]'_z. \tag{A8c}$$

Applying the approximate form of Eq. (A8) to Eqs. (A4) and (A5) yields, after some cumbersome algebra (see Supplemental Material [21])

$$\frac{Q}{Q_0} \approx 1 + \frac{\sigma}{2E}\frac{w^2}{h^2}\left(1 + \frac{\pi^2}{24}\frac{w^2}{L^2} + \frac{1}{2}\sqrt{\frac{\sigma}{3E}}\frac{w^2}{hL}\right)^{-1}, \tag{A9}$$

which reduces to Eq. (1) for a sufficiently long ribbon. In Supplemental Material [21], we show Eq. (1) agrees with numerical simulations for a rectangular ribbon and that the right-hand term can be significantly reduced by filleting the ribbon at clamps. We also extent Eq. (A9) to higher-order torsional modes.

2. Shot noise imprecision of an optical lever

To derive Eq. (2), we consider the optical lever setup shown in Fig. 3, in which a laser beam is reflected off the ribbon and directed toward a split photodiode. The nominal incidence angle is taken to be zero (for illustrative purposes, Fig. 3 is sketched with a nonzero incidence angle), and the laser beam waist (with $1/e^2$ radius w_0) is assumed to coincide with the ribbon. Assuming the laser is in a TEM_{00} Gaussian mode, the optical power difference recorded by the split photodiode is given by the familiar "knife edge" formula

$$\Delta P = P\mathrm{Erf}\left[\frac{\sqrt{2}x}{w(z)}\right], \tag{A10}$$

where x is the lateral displacement of the laser beam from the photodiode midline (in the plane of the photodiode), $w(z) = w_0\sqrt{1 + z^2/z_0^2}$ is the beam width at the photodiode, z is the distance of the photodiode from the ribbon, and $z_0 = \pi w_0^2/\lambda$ is the Rayleigh length of the laser beam.

Equation (2) is obtained by referring laser intensity shot noise

$$S_P^{\mathrm{shot}} = \frac{4\pi\hbar c}{\lambda} P \tag{A11}$$

to an apparent fluctuation of the angular ribbon displacement

$$S_\theta^{\mathrm{imp(shot)}} = \left(\frac{d\Delta P}{dx}\frac{dx}{d\theta}\right)^{-2} S_P^{\mathrm{shot}} = \frac{\hbar c \lambda}{8 w_0^2}\frac{1}{P}\left(1 + \frac{z_0^2}{z^2}\right) \tag{A12}$$

using the small angle approximation $x = 2\theta z$ and the small displacement approximation $(d\Delta P/dx)|_{x \ll w(z)} = \sqrt{8/\pi}[P/w(z)]$. Equation (2) assumes that the photodetector is placed in the far field, $z \gg z_0$.

3. Zero-point displacement spectral density of a torsion oscillator

The zero-point angular displacement spectral density of a torsion oscillator (green curve in Fig. 3) can be expressed as

$$S_\theta^{\mathrm{ZP}}(\omega) = \frac{4\langle\theta_{\mathrm{zp}}^2\rangle}{\gamma_1}|\chi(\omega)|^2, \tag{A13}$$

where $\chi(\omega) \approx [1 + \omega_1^2(\omega - \omega_1)^2/Q_1^2]$ is the relative susceptibility of the oscillator (well approximated by a Lorentzian near resonance $\omega \approx \omega_1$), $\langle\theta_{\mathrm{zp}}^2\rangle = \hbar/2I_1\omega_1$ is

its zero-point displacement variance, and I_1 is its moment of inertia.

To obtain Eq. (3), we define $I_1 = m_1 r_\perp^2$, where m_1 is the effective mass of the fundamental torsion mode of the ribbon defined for a point at the position of maximum transverse displacement, $\phi_y^{\max}$, and $r_\perp = w/2$ is the distance from the torsion axis to the point of maximum displacement. Ignoring mode curvature at the clamps, Eqs. (A7) and (A8) yield

$$m_1 = \frac{\rho \int \phi_y^2(x,y,z)dV}{\phi_{y,\max}^2} = \frac{\rho h w}{3}\int_0^L \sin^2(k_1 z)dz = \frac{m_{\text{phys}}}{6}, \tag{A14}$$

where $m_{\text{phys}} = \rho h w L$ is the physical mass of the ribbon.

[1] L. Sementilli, E. Romero, and W. P. Bowen, *Nanomechanical Dissipation and Strain Engineering*, Adv. Funct. Mater. **32**, 2105247 (2022).

[2] G. I. González and P. R. Saulson, *Brownian Motion of a Mass Suspended by an Anelastic Wire*, J. Acoust. Soc. Am. **96**, 207 (1994).

[3] S. A. Fedorov, N. J. Engelsen, A. H. Ghadimi, M. J. Bereyhi, R. Schilling, D. J. Wilson, and T. J. Kippenberg, *Generalized Dissipation Dilution in Strained Mechanical Resonators*, Phys. Rev. B **99**, 054107 (2019).

[4] Y. Tsaturyan, A. Barg, E. S. Polzik, and A. Schliesser, *Ultracoherent Nanomechanical Resonators via Soft Clamping and Dissipation Dilution*, Nat. Nanotechnol. **12**, 776 (2017).

[5] A. H. Ghadimi, S. A. Fedorov, N. J. Engelsen, M. J. Bereyhi, R. Schilling, D. J. Wilson, and T. J. Kippenberg, *Elastic Strain Engineering for Ultralow Mechanical Dissipation*, Science **360**, 764 (2018).

[6] C. Reinhardt, T. Müller, A. Bourassa, and J. C. Sankey, *Ultralow-Noise* SiN *Trampoline Resonators for Sensing and Optomechanics*, Phys. Rev. X **6**, 021001 (2016).

[7] R. A. Norte, J. P. Moura, and S. Gröblacher, *Mechanical Resonators for Quantum Optomechanics Experiments at Room Temperature*, Phys. Rev. Lett. **116**, 147202 (2016).

[8] D. Hälg, T. Gisler, Y. Tsaturyan, L. Catalini, U. Grob, M.-D. Krass, M. Héritier, H. Mattiat, A.-K. Thamm, R. Schirhagl *et al.*, *Membrane-Based Scanning Force Microscopy*, Phys. Rev. Appl. **15**, L021001 (2021).

[9] S. A. Fedorov, A. Beccari, N. J. Engelsen, and T. J. Kippenberg, *Fractal-Like Mechanical Resonators with a Soft-Clamped Fundamental Mode*, Phys. Rev. Lett. **124**, 025502 (2020).

[10] M. J. Bereyhi, A. Arabmoheghi, A. Beccari, S. A. Fedorov, G. Huang, T. J. Kippenberg, and N. J. Engelsen, *Perimeter Modes of Nanomechanical Resonators Exhibit Quality Factors Exceeding* 10^9 *at Room Temperature*, Phys. Rev. X **12**, 021036 (2022).

[11] T. Quinn, C. C. Speake, H. Parks, and R. Davis, *The BIPM Measurements of the Newtonian Constant of Gravitation, G*, Phil. Trans. R. Soc. A **372**, 20140032 (2014).

[12] R. N. Kleiman, G. K. Kaminsky, J. D. Reppy, R. Pindak, and D. J. Bishop, *Single-Crystal Silicon High-q Torsional Oscillators*, Rev. Sci. Instrum. **56**, 2088 (1985).

[13] J. B. M.Sc., *LXXXIV. The Bifilar Property of Twisted Strips*, London, Edinburgh, Dublin Philos. Mag. J. Sci. **28**, 778 (1914).

[14] S. Schmid, K. D. Jensen, K. H. Nielsen, and A. Boisen, *Damping Mechanisms in High-q Micro and Nanomechanical String Resonators*, Phys. Rev. B **84**, 165307 (2011).

[15] N. Treps, N. Grosse, W. P. Bowen, C. Fabre, H.-A. Bachor, and P. K. Lam, *A Quantum Laser Pointer*, Science **301**, 940 (2003).

[16] Y. Enomoto, K. Nagano, and S. Kawamura, *Standard Quantum Limit of Angular Motion of a Suspended Mirror and Homodyne Detection of a Ponderomotively Squeezed Vacuum Field*, Phys. Rev. A **94**, 012115 (2016).

[17] Y. Michimura and K. Komori, *Quantum Sensing with Milligram Scale Optomechanical Systems*, Eur. Phys. J. D **74**, 126 (2020).

[18] P. Kim, B. Hauer, C. Doolin, F. Souris, and J. Davis, *Approaching the Standard Quantum Limit of Mechanical Torque Sensing*, Nat. Commun. **7**, 13165 (2016).

[19] M. J. Weaver, B. Pepper, F. Luna, F. M. Buters, H. J. Eerkens, G. Welker, B. Perock, K. Heeck, S. de Man, and D. Bouwmeester, *Nested Trampoline Resonators for Optomechanics*, Appl. Phys. Lett. **108**, 033501 (2016).

[20] R. Shaniv, S. K. Keshava, C. Reetz, and C. A. Regal, *Understanding the Quality Factor of Mass-Loaded Tensioned Resonators*, arXiv:2209.01488.

[21] See Supplemental Material at http://link.aps.org/supplemental/10.1103/PhysRevX.13.011018 for comprehensive derivations of all formulas in the main text and the Appendix, details on the measurements shown in Fig. 1–4, and details on nanofabrication.

[22] L. G. Villanueva and S. Schmid, *Evidence of Surface Loss as Ubiquitous Limiting Damping Mechanism in Sin Micro- and Nanomechanical Resonators*, Phys. Rev. Lett. **113**, 227201 (2014).

[23] G. D. Cole, I. Wilson-Rae, K. Werbach, M. R. Vanner, and M. Aspelmeyer, *Phonon-Tunnelling Dissipation in Mechanical Resonators*, Nat. Commun. **2**, 231 (2011).

[24] T. P. Purdy, R. W. Peterson, and C. Regal, *Observation of Radiation Pressure Shot Noise on a Macroscopic Object*, Science **339**, 801 (2013).

[25] D. Mason, J. Chen, M. Rossi, Y. Tsaturyan, and A. Schliesser, *Continuous Force and Displacement Measurement below the Standard Quantum Limit*, Nat. Phys. **15**, 745 (2019).

[26] A. A. Clerk, M. H. Devoret, S. M. Girvin, F. Marquardt, and R. J. Schoelkopf, *Introduction to Quantum Noise, Measurement, and Amplification*, Rev. Mod. Phys. **82**, 1155 (2010).

[27] C. Fabre, J. Fouet, and A. Maître, *Quantum Limits in the Measurement of Very Small Displacements in Optical Images*, Opt. Lett. **25**, 76 (2000).

[28] S. M. Barnett, C. Fabre, and A. Maıtre, *Ultimate Quantum Limits for Resolution of Beam Displacements*, Eur. Phys. J. D **22**, 513 (2003).

[29] M. Aspelmeyer, T. J. Kippenberg, and F. Marquardt, *Cavity Optomechanics*, Rev. Mod. Phys. **86**, 1391 (2014).

[30] J. D. Teufel, T. Donner, M. Castellanos-Beltran, J. W. Harlow, and K. W. Lehnert, *Nanomechanical Motion Measured with an Imprecision below that at the Standard Quantum Limit*, Nat. Nanotechnol. **4**, 820 (2009).

[31] G. Anetsberger, E. Gavartin, O. Arcizet, Q. P. Unterreithmeier, E. M. Weig, M. L. Gorodetsky, J. P. Kotthaus, and T. J. Kippenberg, *Measuring Nanomechanical Motion with an Imprecision below the Standard Quantum Limit*, Phys. Rev. A **82**, 061804(R) (2010).

[32] A. J. Heinrich, W. D. Oliver, L. M. Vandersypen, A. Ardavan, R. Sessoli, D. Loss, A. B. Jayich, J. Fernandez-Rossier, A. Laucht, and A. Morello, *Quantum-Coherent Nanoscience*, Nat. Nanotechnol. **16**, 1318 (2021).

[33] C. A. Putman, B. G. De Grooth, N. F. Van Hulst, and J. Greve, *A Detailed Analysis of the Optical Beam Deflection Technique for Use in Atomic Force Microscopy*, J. Appl. Phys. **72**, 6 (1992).

[34] E. Gavartin, P. Verlot, and T. J. Kippenberg, *Stabilization of a Linear Nanomechanical Oscillator to Its Thermodynamic Limit*, Nat. Commun. **4**, 2860 (2013).

[35] M. Sansa, E. Sage, E. C. Bullard, M. Gély, T. Alava, E. Colinet, A. K. Naik, L. G. Villanueva, L. Duraffourg, M. L. Roukes *et al.*, *Frequency Fluctuations in Silicon Nanoresonators*, Nat. Nanotechnol. **11**, 552 (2016).

[36] M. Wang, R. Zhang, R. Ilic, Y. Liu, and V. A. Aksyuk, *Fundamental Limits and Optimal Estimation of the Resonance Frequency of a Linear Harmonic Oscillator*, Commun. Phys. **4**, 207 (2021).

[37] C. M. Pluchar, A. R. Agrawal, E. Schenk, and D. J. Wilson, *Towards Cavity-Free Ground-State Cooling of an Acoustic-Frequency Silicon Nitride Membrane*, Appl. Opt. **59**, G107 (2020).

[38] P. Sadeghi, M. Tanzer, S. L. Christensen, and S. Schmid, *Influence of Clamp-Widening on the Quality Factor of Nanomechanical Silicon Nitride Resonators*, J. Appl. Phys. **126**, 165108 (2019).

[39] A. Kudrolli and J. Chopin, *Tension-Dependent Transverse Buckles and Wrinkles in Twisted Elastic Sheets*, Proc. Math. Phys. Eng. **474**, 20180062 (2018).

[40] D. Høj, F. Wang, W. Gao, U. B. Hoff, O. Sigmund, and U. L. Andersen, *Ultra-coherent Nanomechanical Resonators Based on Inverse Design*, Nat. Commun. **12**, 5766 (2021).

[41] D. Shin, A. Cupertino, M. H. de Jong, P. G. Steeneken, M. A. Bessa, and R. A. Norte, *Spiderweb Nanomechanical Resonators via Bayesian Optimization: Inspired by Nature and Guided by Machine Learning*, Adv. Mater. **34**, 2106248 (2022).

[42] M. H. de Jong, M. A. t. Wolde, A. Cupertino, P. G. Steeneken, and R. A. Norte, *Mechanical Dissipation by Substrate-Mode Coupling in Sin Resonators*, Appl. Phys. Lett. **121**, 032201 (2022).

[43] J. Steinlechner, C. Krüger, I. W. Martin, A. Bell, J. Hough, H. Kaufer, S. Rowan, R. Schnabel, and S. Steinlechner, *Optical Absorption of Silicon Nitride Membranes at 1064 nm and at 1550 nm*, Phys. Rev. D **96**, 022007 (2017).

[44] X. Chen, C. Chardin, K. Makles, C. Caër, S. Chua, R. Braive, I. Robert-Philip, T. Briant, P.-F. Cohadon, A. Heidmann *et al.*, *High-Finesse Fabry-Perot Cavities with Bidimensional* Si_3N_4 *Photonic-Crystal Slabs*, Light Sci. Appl. **6**, e16190 (2017).

[45] T. Shimoda, Y. Miyazaki, Y. Enomoto, K. Nagano, and M. Ando, *Coherent Angular Signal Amplification Using an Optical Cavity*, Appl. Opt. **61**, 3901 (2022).

[46] T. Purdy, K. Grutter, K. Srinivasan, and J. Taylor, *Quantum Correlations from a Room-Temperature Optomechanical Cavity*, Science **356**, 1265 (2017).

[47] T. P. Purdy, P.-L. Yu, R. W. Peterson, N. S. Kampel, and C. A. Regal, *Strong Optomechanical Squeezing of Light*, Phys. Rev. X **3**, 031012 (2013).

[48] S. Hao and T. Purdy, *Back Action Evasion in Optical Lever Detection*, arXiv:2212.08197.

[49] M. Wang, R. Zhang, R. Ilic, V. Aksyuk, and Y. Liu, *Frequency Stabilization of Nanomechanical Resonators Using Thermally Invariant Strain Engineering*, Nano Lett. **20**, 3050 (2020).

[50] P. Sadeghi, A. Demir, L. G. Villanueva, H. Kähler, and S. Schmid, *Frequency Fluctuations in Nanomechanical Silicon Nitride String Resonators*, Phys. Rev. B **102**, 214106 (2020).

[51] A. Beccari, D. A. Visani, S. A. Fedorov, M. J. Bereyhi, V. Boureau, N. J. Engelsen, and T. J. Kippenberg, *Strained Crystalline Nanomechanical Resonators with Quality Factors above 10 Billion*, Nat. Phys. **18**, 436 (2022).

[52] R. Middlemiss, A. Samarelli, and D. e. a. Paul, *Measurement of the Earth Tides with a MEMS Gravimeter*, Nature (London) **531**, 614 (2016).

[53] S. Tang, H. Liu, S. Yan, X. Xu, W. Wu, J. Fan, J. Liu, C. Hu, and L. Tu, *A High-Sensitivity MEMS Gravimeter with a Large Dynamic Range*, Microsyst. Nanoeng. **5**, 45 (2019).

[54] A. Mustafazade, M. Pandit, and C. Zhao, *A Vibrating Beam MEMS Accelerometer for Gravity and Seismic Measurements*, Sci. Rep. **10**, 10415 (2020).

[55] B. de Saint-Venant, *Mémoire sur la Torsion des Prismes*, Mémoires des Savants étrangers **14.233**, 560 (1855).

[56] J. Chopin and R. T. D. Filho, *Extreme Contractility and Torsional Compliance of Soft Ribbons under High Twist*, Phys. Rev. E **99**, 043002 (2019).

[57] E. J. Sapountzakis, *Bars under Torsional Loading: A Generalized Beam Theory Approach*, ISRN Civ. Eng. **2013**, 916581 (2013).

[58] A. E. H. Love, *A Treatise on the Mathematical Theory of Elasticity* (Cambridge University Press, Cambridge, England, 2013).